

Microlensing of radially pulsating stars

Sedighe Sajadian^{1*}, Richard Ignace^{2†*}

¹*Department of Physics, Isfahan University of Technology, Isfahan 84156-83111, Iran*

²*Department of Physics & Astronomy, East Tennessee State University, Johnson City, TN 37614, USA*

Accepted XXX. Received YYY; in original form ZZZ

ABSTRACT

Here, we study the microlensing of radially pulsating stars. Discerning and characterizing the properties of distant, faint pulsating stars is achievable through high-cadence microlensing observations. Combining stellar variability period with microlensing gives the source distance, type, and radius and helps better determine the lens parameters. Considering periodically variations in their radius and surface temperature, their microlensing light curves are resulted from multiplication of the magnification factor with variable finite size effect by the intrinsic brightness curves of pulsing source. The variable finite source size due to pulsation can be significant for transit and single microlensing and while caustic-crossing features. This kind of deviation in the magnification factor is considerable when the ratio of the source radius to the projected lens-source distance is in the range of $\rho_*/u \in [0.4, 10]$ and its duration is short and in the same order of the time of crossing the source radius. Other deviations due to variable source intensity and its area make colored and periodic deviations which are asymmetric with respect to the signs of pulsation phase. The positive phases makes deviations with larger amplitude than negative phase. These deviations dominate in filters with short wave lengths (e.g., B -band). The position of magnification peaks in microlensing of variable stars varies and this displacement differs in different filters.

Key words: gravitational lensing; micro, (stars:) pulsars; general, methods: numerical

1 INTRODUCTION

Most stars display some variation of brightness with time; for instance, even the Sun is a variable star, but its luminosity changes by only around 0.1% over the eleven year solar cycle (Fröhlich 2006). Variable stars can be classified into two basic categories: extrinsic variables such as binary eclipsing stars (see, e.g., Jetsu & Porceddu 2015), and intrinsic variables such as pulsating variable stars (see, e.g., Zhevakin 1963; Cox 1980; Pel 1985; Saio 1993; Carroll & Ostlie 1996). The variation in the brightness of radially pulsating stars arises from periodic expansion and contraction, with consequent variations in the rate at which radiation emerges from the stellar surface. These stars are mostly bright giants or supergiants, much more luminous than the Sun, and their periods range from days to months. They are classified according to their periods of variation and the shape of their light curves, as reflective of evolutionary stages and initial mass (Catelan & Smith 2015; Percy 2007). For radially pulsating stars, there is a relation between their luminosity and the period of their variation, the so-called Leavitt's law, which makes radial pulsators such as Cepheid and RR Lyrae stars standard candles (see, e.g., Benedict et al. 2002; Turner 2010). The relation between the pulsation characteristics, stellar evolu-

tion and stellar properties, along with their use as standard candles, makes the detection and detailed study of radial pulsators important to astrophysics, even beyond stellar astrophysics (see, e.g., Majaess et al. 2009). For instance, the discovery of Leavitt's Law and identification of Cepheids in other galaxies led to the Hubble expansion law, which completely changed our perspective of the Universe (Hubble & Humason 1931; Hubble 1929). To date, more than 55,000 confirmed variable stars can be found in *General Catalogue of Variable Stars (GCVS)*¹ (Samus et al. 2009, 2017).

Identifying pulsating stars requires intensive observations over several decades (Udalski et al. 1999; Soszynski et al. 2008; Skowron et al. 2019). However, some of variable stars, e.g., low-amplitude variables, short period ones and irregular variables, are difficult to identify and classify. Spectroscopic observations from these puzzling variables can reveal their types and properties (Kinman & Brown 2010; Pietrukowicz et al. 2015, 2017). But spectroscopy is helpful only for bright source stars. Distant (and therefore faint), low-amplitude variable stars can become observable through brightness magnification during gravitational microlensing events. Macrolensing refers to the ability to detect multiple images from gravitational lensing, whereas microlensing refers to the limit when the multiple images are not resolved, yet do lead to

* E-mail: s.sajadian@iut.ac.ir

† E-mail: ignace@etsu.edu

¹ <http://www.sai.msu.su/gcvs/gcvs/>

brightness variations. Macrolensing occurs on cosmological scales, whereas microlensing refers to lensing masses like stars for distance scales relevant to the Milky Way and Local Group (Schneider et al. 1992; Fu & Shu 2005). Currently, monitoring efforts to detect gravitational microlensing events are conducted toward the Galactic Bulge (Mróz et al. 2019; Bond et al. 2001; Kim et al. 2018). A background source star is magnified when nearly aligned with a foreground mass (Einstein 1936; Paczynski 1986; Wambsganss 2006). Microlensing has been employed in recent years as a technique for detecting extra-solar planets owing to how their masses modify stellar light curves from normal lensing events associated with stellar masses (Mao & Paczynski 1991; Gould & Loeb 1992; Gaudi 2012).

The brightness magnification from microlensing can help with discerning short and/or low-amplitude variations in the variable star light curve which is intrinsically faint. Microlensing is the only method for highlighting small stellar perturbations, even time-variable ones (see, e.g., Bennett & Rhie 1996). Through magnifying faint stars that are pulsators, we can better identify the pulsational period to constrain the absolute magnitude of the source star and determine the star's distance. Determining the source distance, its type, and radius independently in microlensing events helps better constrain the mass and distance of the lens object.

Microlensing surveys, such as OGLE, MOA, and KMTNet, generally have not emphasized pulsating variables as source stars of microlensing events (Assef et al. 2006). However, one example of microlensing of a pulsating star was discovered recently (Li et al. 2019). For this microlensing event, OGLE-2017-BLG-1186, the source star was a bright and variable red giant. Its amplitude of variation was high enough so that asteroseismology from ground-based data revealed the pulsation curve and as a result its stellar type, average source size, and distance. Measuring the finite source size (Gould 1994; Witt & Mao 1994; Nemiroff & Wickramasinghe 1994) carefully in addition to the parallax effect provides a solution for the mass and distance of the lensing star. However, the analysis of this event did not take account of the variation in the physical extent of the star. Clearly, radial pulsations mean the source radius is not fixed. Here, we investigate the effect of varying finite source size for the lensing magnification.

In this paper, Section 2 provides a formalism for microlensing of radially pulsating stars. There we introduce an overall magnification factor as depending on the time varying size and temperature of the star along with how the traditional magnification factor is averaged of the finite stellar size. We explore the contributions of these different effects. In Section 3 results for single-lens events are presented and discussed. Then results for the binary-lens scenario are given in Section 4. We summarize these results and provide concluding remarks in the last section.

2 FORMALISM FOR MICROLENSING OF RADIAL PULSATING STARS

Radial pulsating stars vary in both effective surface temperature and radius leading to periodic modulations of their observed specific fluxes (Cox 1980). While the flux and effective temperature curves have similar phases versus time, variations in the radial extent of the atmosphere will lag these by around quarter in pulsational phase. Since our objective is to explore basic observable consequences from the microlensing of pulsating stars, we adopt a somewhat simplistic for atmospheric variations of a radial pulsating star. We choose periodically sinusoidal functions for variations

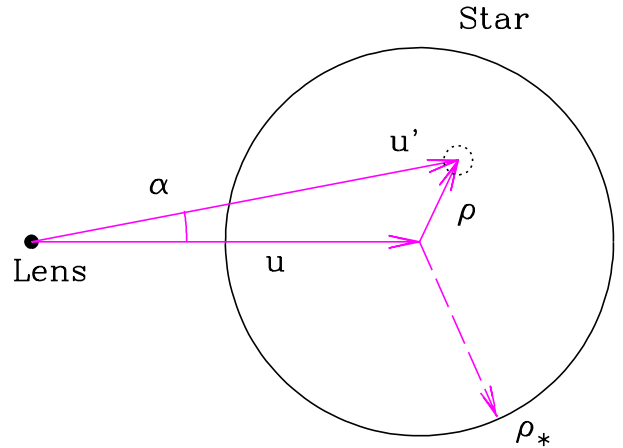


Figure 1. Figure represents the lens plane which contains the projected source surface with the radius ρ_* . The coordinates of the source center and an arbitrary point of it with respect to the lens location is specified as $(u, 0)$ and $(u' \cos \alpha, u' \sin \alpha)$, respectively.

of the stellar radius, R_* , and effective stellar temperature, T_* , as follows (Bryce 2001):

$$R_*(t) = \bar{R} + \delta_R \sin[\omega(t - t_p) + \phi_0], \text{ and} \quad (1)$$

$$T_*(t) = \bar{T} + \delta_T \sin[\omega(t - t_p)], \quad (2)$$

where \bar{R} and \bar{T} are the average radius and effective temperature of the source star of one pulsational cycle, t_p is an arbitrary time offset, $\omega = 2\pi/P$ is the pulsating angular velocity with P the period of pulsation, and ϕ_0 is the phase difference between the radius and temperature curves with $\phi_0 \approx -\pi/2$. Then δ_R and δ_T are relative amplitude factors for the variation of radius and temperature, respectively.

We further treat the star as a blackbody for the specific intensity of emission from the atmosphere, with $B_\lambda(T_*)$:

$$B_\lambda(T_*) = \frac{8\pi hc^2}{\lambda^5} \frac{1}{\exp\left(\frac{hc}{kT_*\lambda}\right) - 1}, \quad (3)$$

where λ is the wavelength, c is the speed of light, k is the Boltzmann constant, h is the Planck constant, and B_λ is given in units of W.m^{-3} . The time-dependent passband flux of the source star received by the observer becomes,

$$F_*(t) = \left[\frac{R_*(t)}{D_s} \right]^2 \times \pi I_*(t), \quad (4)$$

where D_s is the distance to the source star, and the passband dependence enters through

$$I_*(t) = \int_0^\infty d\lambda K(\lambda - \lambda_0) B_\lambda(T_*). \quad (5)$$

This “passband intensity” emitted from the stellar surface is associated with an observational filter characterized by wavelength λ_0 . The throughput of the filter, $K(\lambda - \lambda_0)$, is taken to have unit area when integrated over wavelength. Note that in keeping with the theme of a simplified model, the star is taken to have no limb

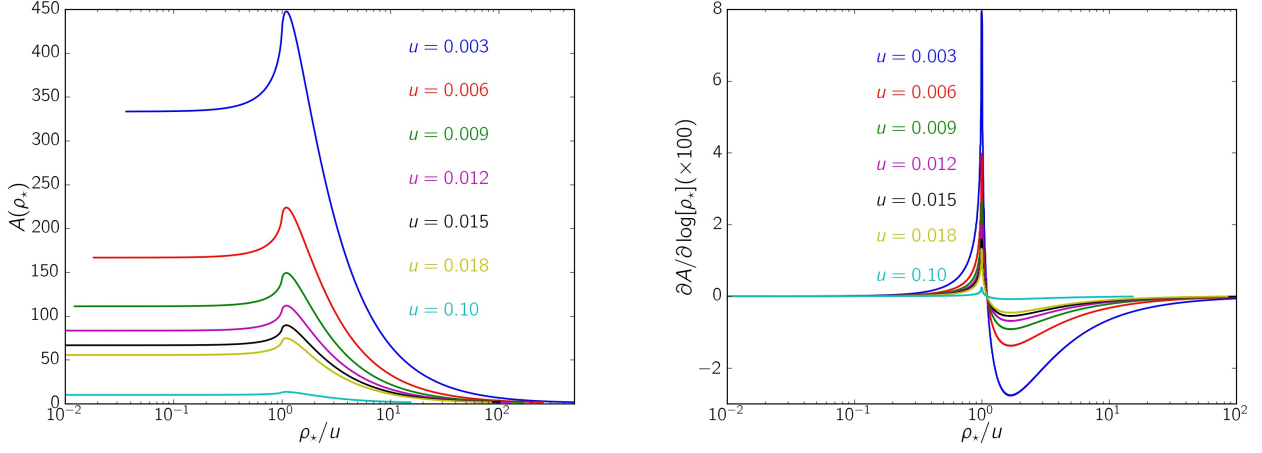


Figure 2. The microlensing magnification factor $A(\rho_*, u)$ (left panel) and its derivative (right panel) versus ρ_*/u for different values of u , the lens distance from the source center normalized to the Einstein radius.

darkening. However, equation (5) could be modified to include the effect of limb darkening.

To evaluate the amplification factor from microlensing of a radial pulsating star, Figure (1) illustrates the geometry in the plane of the sky. The star is taken to have angular radius $\theta_* = R_*(t)/D_s$. However, it is convenient to express angular separations relative to the angular Einstein radius, the latter being $\theta_E = R_E/D_l$, where R_E is the linear Einstein radius in the lens plane, and D_l is the distance to the lens. A stellar radius parameter introduces as

$$\rho_* = \theta_*/\theta_E. \quad (6)$$

Related, we define θ as the angular separation in the sky between the lens and the center of star, and we introduce

$$u = \theta/\theta_E = \sqrt{u_0^2 + \left(\frac{t - t_0}{t_E}\right)^2}, \quad (7)$$

as the lens-source separation normalized to the Einstein radius and projected on the lens plane. Here, u_0 , is the minimum separation (i.e., impact parameter) between the lens and source on the lens plane and normalized to the Einstein radius. Correspondingly, t_0 is the time of closest approach when u_0 is achieved. The Einstein crossing time, $t_E = R_E/v_t$, is the time to cross the Einstein radius given the lens-source transverse velocity v_t . If the source radius is negligible in comparison with u , i.e., $u \gg \rho_*$, the magnification factor for the single lens is given by:

$$A(u) = \frac{u^2 + 2}{u\sqrt{u^2 + 4}}. \quad (8)$$

The curve of this magnification factor versus time is known as the simple Paczyński light curve (Paczynski 1986; Witt & Mao 1994). For microlensing that takes account of the finite stellar size, we define θ' and $u' = \theta'/\theta_E$ which are dummy variables for determining the amplification factor $A(u, \rho_*)$, with

$$A(u, \rho_*) = \frac{\int A(u') I(u', \alpha) u' du' d\alpha}{\int I(u') u' du' d\alpha}, \quad (9)$$

and A is given by Equation (8). Note that in our treatment that

currently ignores either limb darkening or non-radial pulsations, $I(u', \alpha) = I_*(t)$, and the above expression simplifies to

$$A(u, \rho_*) = \frac{1}{\pi \rho_*^2} \int A(u') u' du' d\alpha. \quad (10)$$

Note that $A(u, \rho_*) \geq 1$ has no units owing to normalization by the unlensed brightness of the star. The case of $A = 1$ represents no lensing. The case of $u \gg \rho_*$ is the traditional case of point lensing of a point-like star. But when $u \lesssim \rho_*$, the amplification of the star changes relative to treating the star as a point source. While A is implicitly time-dependent by virtue of this surface averaging over a star whose extent is varying, we need another factor to represent the *observed* amplification of the source, which we define as

$$A_o(t) \equiv \frac{I_*(t)}{\bar{I}} \left[\frac{R_*(t)}{\bar{R}} \right]^2 A(u, \rho_*), \quad (11)$$

where the time-averaged passband intensity is given by

$$\bar{I} = \frac{1}{P} \int_0^P I_*(t) dt. \quad (12)$$

The intrinsic variation in the stellar temperature and its radius makes time-dependent perturbations in the magnification factor.

2.1 General characterizations

According to equation (11), there are three sources of time-dependent variations associated with the microlensing of radial pulsators (i.e., in addition to the relative motion between the lens and source): (i) the finite source size ρ_* which changes the magnification factor, (ii) the source radius which changes the emitting area of the source by $(R_*(t)/\bar{R})^2$, and (iii) the intrinsic intensity of the source star owing to the variation in the stellar temperature $I_*(t)/\bar{I}$. As a result, the observed microlensing light curve will deviate from a standard Paczyński light curve (c.f., Eqn 8). To understand when the pulsation-induced deviation in the observed magnification factor becomes significant, we investigate each of these 3 factors separately. For this initial study, we focus on the single-lens case.

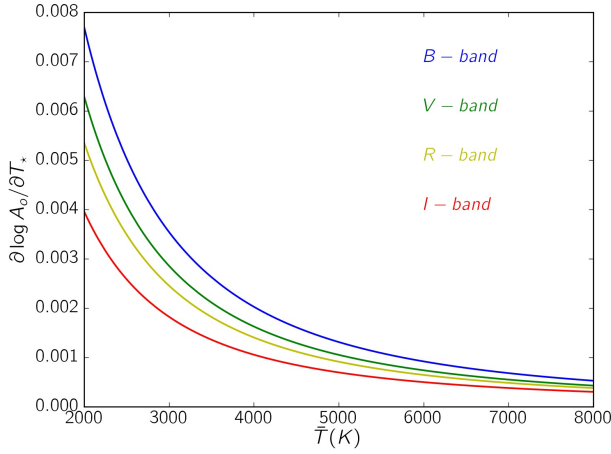


Figure 3. The partial derivatives of the observed magnification factor A_o with respect to T_* which is normalized to the observed magnification factor versus the source surface temperature.

(i) $\mathbf{A}(\rho_*(t), \mathbf{u})$: The lefthand side of Figure (2) shows the magnification factor A as plotted against ρ_*/u for several values of lens-star separations, u . Maxima are found numerically to occur when $u = \rho_*/1.1 = 0.91\rho_*$. This corresponds to where the projected position of the lens is slightly interior to the projected source surface. We calculated the magnification factor with finite source size using the RT-model developed by V. Bozza (Bozza et al. 2018; Bozza 2010; Skowron & Gould 2012). The magnification factor decreases for $\rho_*/u > 1.1$ and the calculation approaches that of the point-lens with point-source as the finite size of the star becomes diminishingly relevant. For $\rho_*/u < 1.1$, the magnification factor decreases somewhat but then approaches a near-constant value as $\rho_* \rightarrow 0$.

To investigate the rate of variation of the magnification factor due to the variation in ρ_* , we differentiate the magnification factor with respect to ρ_* and plot the result in the rightside panel of Figure (2). The sharp positive peaks of $\partial A/\partial \ln \rho_*$ occur when $\rho_* = u$ (turning point), and the derivative changes sign when $\rho_* = 1.1u$. If the lens distance from the source center is larger than $\rho_*/1.1$, this derivative, $\partial A/\partial \rho_*$, is positive, such that increasing the source radius enhance the magnification factor. Contrastly, when $u < \rho_*/1.1$, the derivative is negative. In conclusion, the magnification factor displays its greatest response to the variable size of the star when $\rho_* \sim u$.

The derivative normalized to the magnification factor is related to the relative deviation in the observed magnification factor as:

$$\frac{\partial \ln A_o}{\partial \rho_*} = \frac{\partial \ln A}{\partial \rho_*}. \quad (13)$$

This relative deviation in A_o is small when the averaged source radius is larger than $\sim 10u$ and less than $0.4u$. Hence, the considerable deviation happens when $0.4 \lesssim \rho_*/u \lesssim 10$. The time scale of this deviation is in the same order of magnitude of $t_* = t_E \rho_*$, the time of crossing the source radius. In order to estimate the value of t_* , consider as an example a microlensing event toward the Galactic Bulge with typical parameters: a Bulge distance $D_s = 8.5$ kpc, a lens distance $D_l = 6$ kpc, a lens mass $M_l = 0.3M_\odot$, a transverse

velocity $v_t = 120$ km/s, a Bulge giant star radius $R_* = 10R_\odot$ which results in $R_E = 2.1$ au, $t_E = 29.9$ days, and $\rho_* = 0.02$. These parameters then yield $t_* = 0.5$ day. During this time scale, measuring the pulsation period is impossible, unless $p \lesssim t_*$ (which is rare).

(ii) \mathbf{R}_*^2 : The area of pulsating source stars changes with time which makes variable intrinsic luminosity for the source star. The relative derivative of the observed magnification factor with respect to the source radius is given by:

$$\frac{\partial \ln A_o}{\partial R_*} = + \frac{2}{R_*}. \quad (14)$$

When the source radius is large, the relative rate of variation in the magnification is small, and vice versa. Also, $\partial A_o/\partial R_*$ is positive always, i.e., by increasing R_* the observed magnification factor increases and vice versa. For stars of relatively small angular size, the derivative of the observed magnification factor with respect to R_* is large, but its derivative with respect to ρ_* is large only when $u \sim \rho_*$.

(iii) $\mathbf{I}_*(t)$ The intrinsic intensity from pulsating source stars derives its variability from the surface temperature. The relative derivative of the magnification with respect to the stellar surface temperature is:

$$\frac{\partial \ln A_o}{\partial T_*} = \frac{\partial \ln I_*}{\partial T_*}. \quad (15)$$

This function is plotted in Figure (3) against stellar temperature in different standard Johnson filters BVRI. The variation in the stellar surface temperature makes the observed magnification factor change differently in various filters. The largest relative variations in the observed magnification factor due to variation in the stellar temperature happens in the B-band. For hotter stars the BVRI are more in the Rayleigh-Jeans tail, for which the above equation approaches a T_*^{-1} dependence. On the Wien side for quite cool stars, the normalized derivative approaches T_*^{-2} , which is much steeper. Hence, temperature variability leads to stronger effects in the magnification factor for cooler stars.

Generally, T_* , R_* , and ρ_* all change with time, simultaneously, but not necessarily in phase. The relative rate of variation in the observed magnification factor with time can be written as a summation of its derivatives involving equations (13), (14) and (15) as follows:

$$\begin{aligned} \frac{\partial \ln A_o}{\partial t} &= \left[\frac{\partial \ln A}{\partial \rho_*} \delta_\rho + \frac{2}{R_*} \delta_R \right] \omega \cos[\omega(t - t_p) + \phi_0] \\ &+ \frac{\partial \ln I_*}{\partial T_*} \delta_T \omega \cos[\omega(t - t_p)], \end{aligned} \quad (16)$$

where $\delta_\rho = (\delta_R D_l)/(R_E D_s)$ is δ_R projected onto the lens plane and normalized to the Einstein radius. Accordingly, the derivative (the rate of perturbations) in the observed magnification factor increases linearly with ω , δ_R and δ_T in addition to the mentioned effects. Note that the sign of the relative derivative in the observed magnification factor depends on the variation phase.

2.2 Small and periodic perturbations

For the small variations in the source radius and its temperature, we can use the Taylor expansions in time around their average values as following:

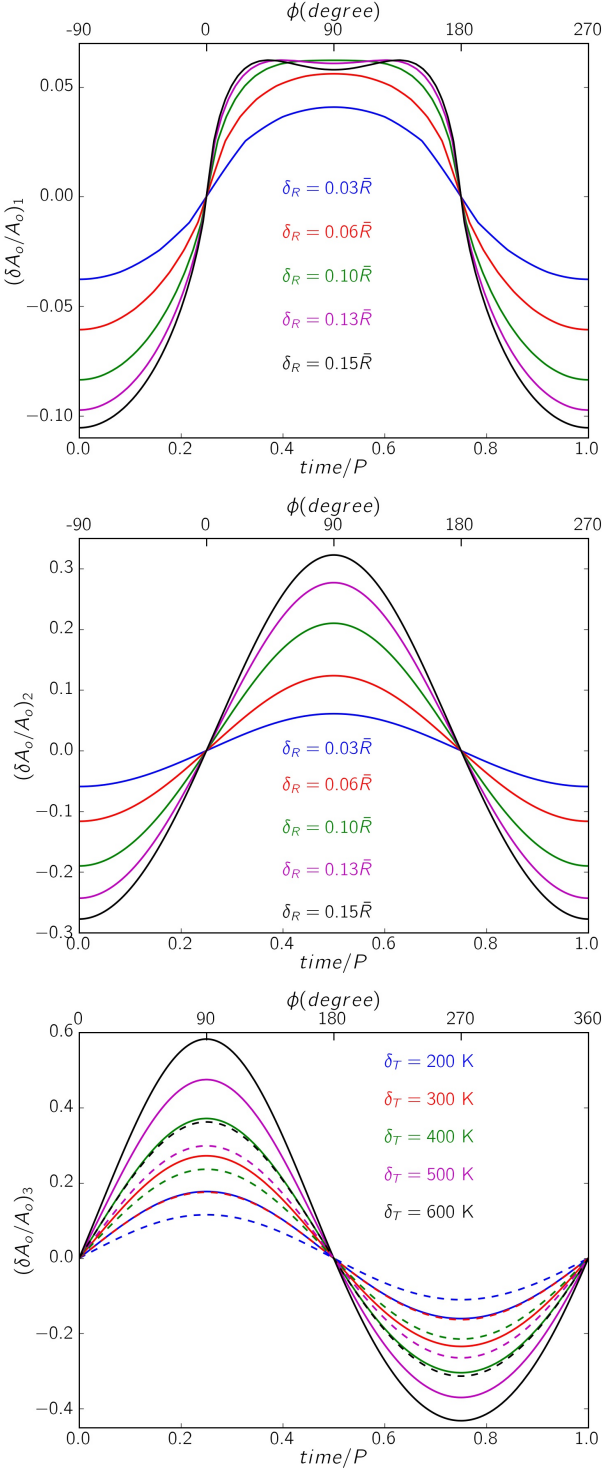


Figure 4. The relative deviations in the observed magnification factor due to the deviation in A (top plot), R_\star^2 (middle plot) and I_\star (bottom plot) during one period for different amplitudes δ_R and δ_T . In the last plot, the solid and dashed curves are in filters V and I -bands.

$$\begin{aligned} A(u, \rho_\star) &= A(u, \bar{\rho}_\star) + A'(t) \times [\rho_\star(t) - \bar{\rho}_\star], \\ R_\star &= \bar{R} + R'_\star(t) \times [R_\star(t) - \bar{R}], \\ I_\star &= \bar{I} + I'_\star(t) \times [I_\star(t) - \bar{I}]. \end{aligned} \quad (17)$$

By substituting these expansions into equation (11), and considering only first-order terms, the relative deviation in the observed magnification factor becomes:

$$\frac{\delta A_o}{A_o} = \frac{\delta A}{A} + \frac{\delta R_\star^2}{R_\star^2} + \frac{\delta I_\star}{I_\star} = \left(\frac{\delta A_o}{A_o} \right)_1 + \left(\frac{\delta A_o}{A_o} \right)_2 + \left(\frac{\delta A_o}{A_o} \right)_3. \quad (18)$$

The relative variation in the observed magnification factor is the sum of these factors for small amplitudes of variations. These relative variations are plotted in the three panels of Figure (4) versus time for one pulsation period. The fixed parameters selected for these plots are $u = 0.007$, $\bar{R} = 5R_\odot$, $\bar{\rho}_\star = 0.0069$, and $\bar{T} = 5600$ K. In the bottom plot, the solid and dashed curves are for the V and I -band filters, respectively. These variations are calculated with respect to average values (at the baseline) and so they are not derivatives. Hence, the scales on y -axes of the different panels can be compared directly for how the different factors contribute to variability.

(*) : For the first plot, when the source radius is increasing (when the ϕ changes from 0 up to 180), at times $0.25P$ and $0.75P$, the lens distance is $u \sim \rho_\star$, corresponding to when the maximum rates of deviations in the magnification factor occur. For these events the maximum deviations in the magnification factor happens when the lens is outside the source radius and the source size is minimum. For a fixed u , decreasing and increasing ρ_\star has an asymmetric effect on the magnification factor.

(*) : Variations in R_\star changes the projected source area with significantly larger impact on the total magnification as compared to variation in ρ_\star , even when $u \sim \rho_\star$. Sign changes between the top and the middle panels are correlated.

(*) : Deviations in the observed magnification factor due to $\delta_T \sim 200$ K and $\delta_R \sim 0.06\bar{R}$ are at similar orders of magnitude (i.e., 0.1). Likewise, pulsations with $\delta_T = 400$ K and $\delta_R = 0.15\bar{R}$ produce similar levels of variability in the observed magnification factor. However, our choice of $\phi_0 = -\pi/2$ leads to a quarter shift in phase for the sign change between the upper two panels and the lowest one for temperature.

(*) : According to the bottom plot, increasing the stellar temperature produce a larger amplitude of deviation in the magnification as compared to decreasing the stellar temperature. This occurs because in the Taylor expansion for negative perturbation, the terms with odd power will be negative whereas others are positive and will eliminate each other; then for a positive perturbation, all powers have the same signs.

(*) : Increasing the stellar radius results in a larger deviation of the magnification as compared to decreasing it (see the middle plot). In considering the variational term for R_\star :

$$\left(\frac{\delta A_o}{A_o} \right)_2 = \delta_R \sin(\omega(t - t_p) + \phi_0) [2 + \sin(\omega(t - t_p) + \phi_0)]. \quad (19)$$

The two terms in square brackets will add constructively if

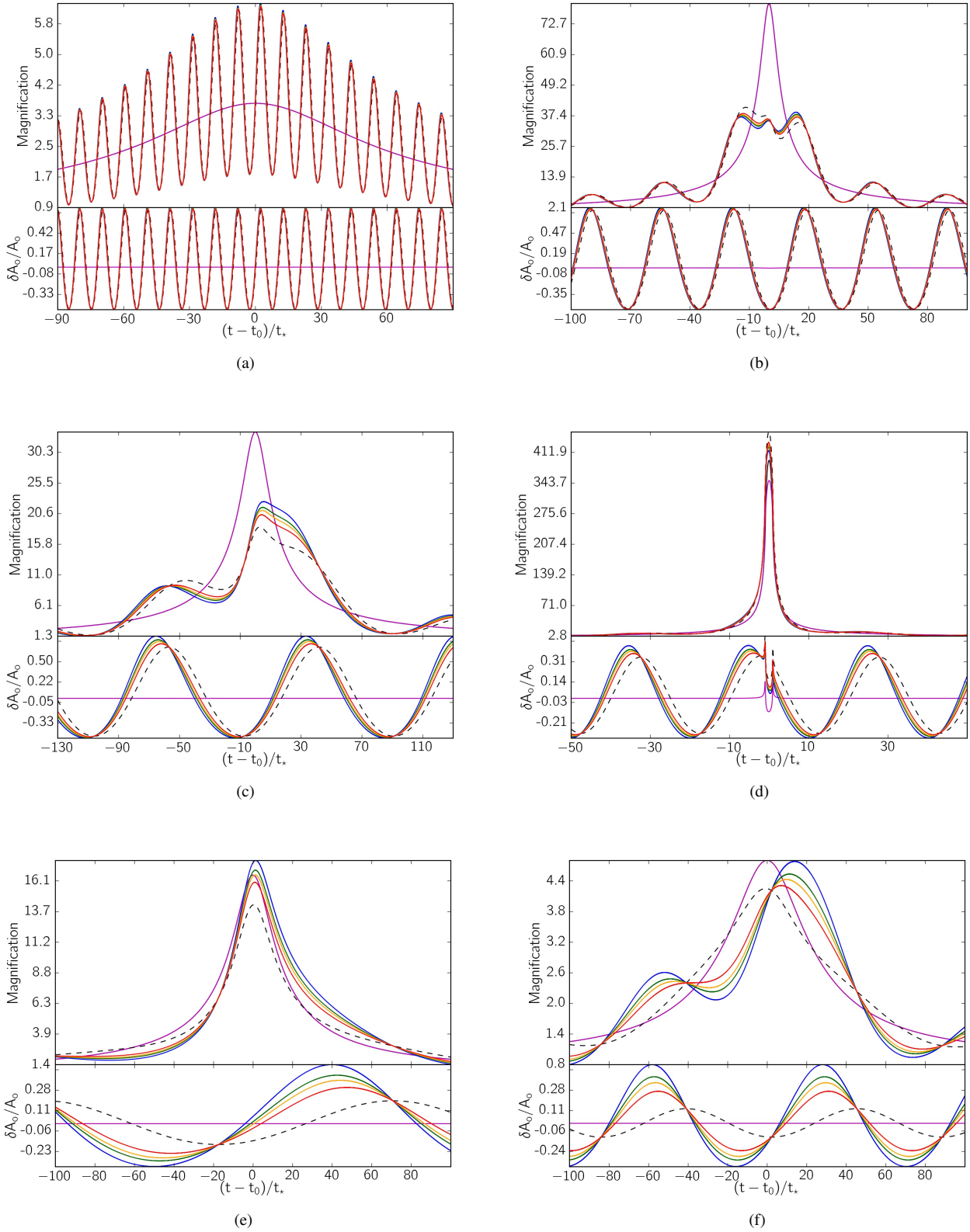


Figure 5. Examples of microlensing light curves of radial pulsating stars. The parameters of each light curve can be found in each row of Table (1). The net microlensing light curve without pulsating effects are plotted with solid black curve. The light curves with considering just variation in ρ_* are shown in solid magenta curves. The dashed black curves represent the microlensing light curves with applying the changes in ρ_* as well as the factor of variation of source area, i.e., $A(\rho_*) \left(\frac{R_*(t)}{R}\right)^2$. The curves of the observed magnification factor, A_o , in B , V , R and I —bands are represented by blue, dark-green, orange and red solid curves, respectively. The residuals $\delta A_o / A_o = (A_o(\rho_*) - A(\bar{\rho}_*)) / A(\bar{\rho}_*)$ are shown at the bottom of each light curve.

Table 1. Table contains the parameters used to make microlensing light curves shown in Figures (5) and (6).

	δ_R (R_*)	δ_T (K)	P (day)	t_P (day)	u_0	ρ_*	t_E (day)	ξ (deg)	d (R_E)	q
5(a)	0.30	144.3	1.42	3.2	0.281	0.006	23.6	—	—	—
5(b)	0.33	240.9	1.90	−1.7	0.012	0.003	18.3	—	—	—
5(c)	0.30	223.1	7.48	2.9	0.029	0.003	23.3	—	—	—
5(d)	0.16	214.9	1.10	1.5	0.002	0.005	7.6	—	—	—
5(e)	0.09	382.7	6.90	−0.7	0.060	0.006	6.4	—	—	—
5(f)	0.06	381.7	5.90	0.3	0.210	0.011	5.9	—	—	—
6(a)	0.19	172.7	2.31	23.9	0.062	0.013	56.5	0.9	0.89	0.71
6(b)	0.32	107.9	12.88	9.4	0.085	0.020	10.9	17.5	0.68	0.33
6(c)	0.24	383.2	4.63	6.5	0.006	0.053	12.9	−9.5	1.03	0.73
6(d)	0.13	285.7	4.11	23.9	0.354	0.001	39.4	268.2	0.74	0.39

$\sin[\omega(t - t_p) + \phi_0] > 0$, but when the sinusoidal term is negative, the amplitude of variation will be reduced.

In order to examine the overall perturbations in microlensing light curves due to stellar pulsation, we simulate the single and binary microlensing light curves from pulsing source stars in the next sections.

3 SINGLE-LENS MICROLENSING OF PULSING STARS

Figure (5) shows six simulated microlensing light curves of radial pulsating stars. The parameters which have significant impacts on the light curves are reported in Table (1). Light curves without pulsation are plotted with solid black curve (behind the magenta curve). Light curves with only variations in ρ_* are plotted as solid magenta; those that include variations of ρ_* and $(R_*(t)/\bar{R})^2$ combined are shown as dashed black curves. Curves for the observed magnification factor A_o in B , V , R and I —bands are shown by blue, dark-green, orange, and red solid curves, respectively. The residuals with respect to the solid black curves, $(A_o(\rho_*) - A(\bar{\rho}_*))/A(\bar{\rho}_*) = \delta A_o/A_o$, are plotted in the bottom panels of each light curve.

We first assume that the lens impact parameter, i.e., u_0 , is larger than the source radius ($u_0 > \bar{\rho}_*$) (i.e., not transit of the star by the lens). In that case, microlensing only perturbs the pulsation curve. The deviation in the variability due to microlensing depends on the period and the width of the microlensing light curve. If $u_0 t_E \gtrsim P$, several variable pulses magnify due to lensing, as in Figure 5(a). On the other hand, if P is the same order as the light curve's width, one or two pulses will be perturbed. In the case that the minimum of the intrinsic stellar intensity happens at the time of closest approach, the deviation will be maximum (see Figs 5(b) and 5(c)).

Now we consider microlensing events with smaller lens impact parameter $u_0 \leq 10\rho_*$. For these events, since the magnification is high, the pulsation will produce perturbations on the main light curve. Indeed, the general form of the microlensing light curve does not change during lensing, so we interpret this as perturbation on the microlensing light curve due to pulsations. According to the previous section, the variability of ρ_* will be significant only for transit microlensing events ($\rho_* \gtrsim u_0$). In that case, the solid magenta curves which isolate the effect of the magnification factor dependence on ρ_* as a function of time will be deviate from solid black curve, as shown in Figure 5(d), otherwise the solid magenta and dashed black curves are always coincident. This point can be inferred from the right panel of Figure (2). In Figure 5(d) because

of high magnification factor, the light curves in different filters are similar.

We note that in the analysis of the first microlensing event of a pulsating source star reported by Li et al. (2019), the effect of a varying ρ_* was not considered. In this event, although the pulsation period which was estimated at ~ 9 days is longer than $t_* \sim 3.7$ days, the lens was crossing the source surface ($u_0 < \rho_*$). Consequently, variation in ρ_* alters the slope of the light curve and its peak value. By fixing ρ_* , a wrong estimate for the lens impact parameter could result.

If the source is at neither maximum nor minimum at the time of closest approach between the lens and the source center, the two sides of the microlensing light curve will not be symmetric with respect to t_0 . Figures 5(e) and 5(f) emphasize the resulting asymmetry that can result.

When δ_T is large ($\gtrsim 200$ K), the difference between light curves for different filters can be significant (e.g., compare Figs. 5(c) and 5(e)). Generally, in the microlensing of pulsating stars, the time of the maximum magnification will not be exactly t_0 , unless the peak of the source intrinsic brightness happens exactly at the time of the closest approach (which is rare). And the modified maximum times are not the same in different filters. Since the perturbation on the light curve due to pulsation is higher for shorter wavelengths, the light curves in the B —band will show a greater displacement in the time of the magnification peak (from t_0) as compared with other filters. This point is shown in Figures 5(e) and 5(f). The phase difference between the residual curves (dashed black ones and colored solid ones) vanishes as δ_T decreased. For large values of δ_T (e.g., $\gtrsim 200$ K), the phase differences are enhanced.

4 BINARY MICROLENSING OF PULSING STARS

Among reported microlensing events, a remarkable fraction involve binary lenses with caustic-crossing features (Wyrzykowski et al. 2015; Alcock et al. 2000). When a background source has a caustic crossing, the magnification factor enhances significantly so that small perturbations on the stellar surface or in its flux can be greatly magnified and detectable (see, e.g., Schneider et al. 1992; Gaudi 2012). Here, we study if the pulsing signatures from source stars can be revealed in caustic crossing features, or when the source stars pass close to the caustic curves.

Figure (6) shows four examples of simulated binary microlensing events involving pulsing source stars. Their characterizations are the same as Figure (5), with model parameters provided

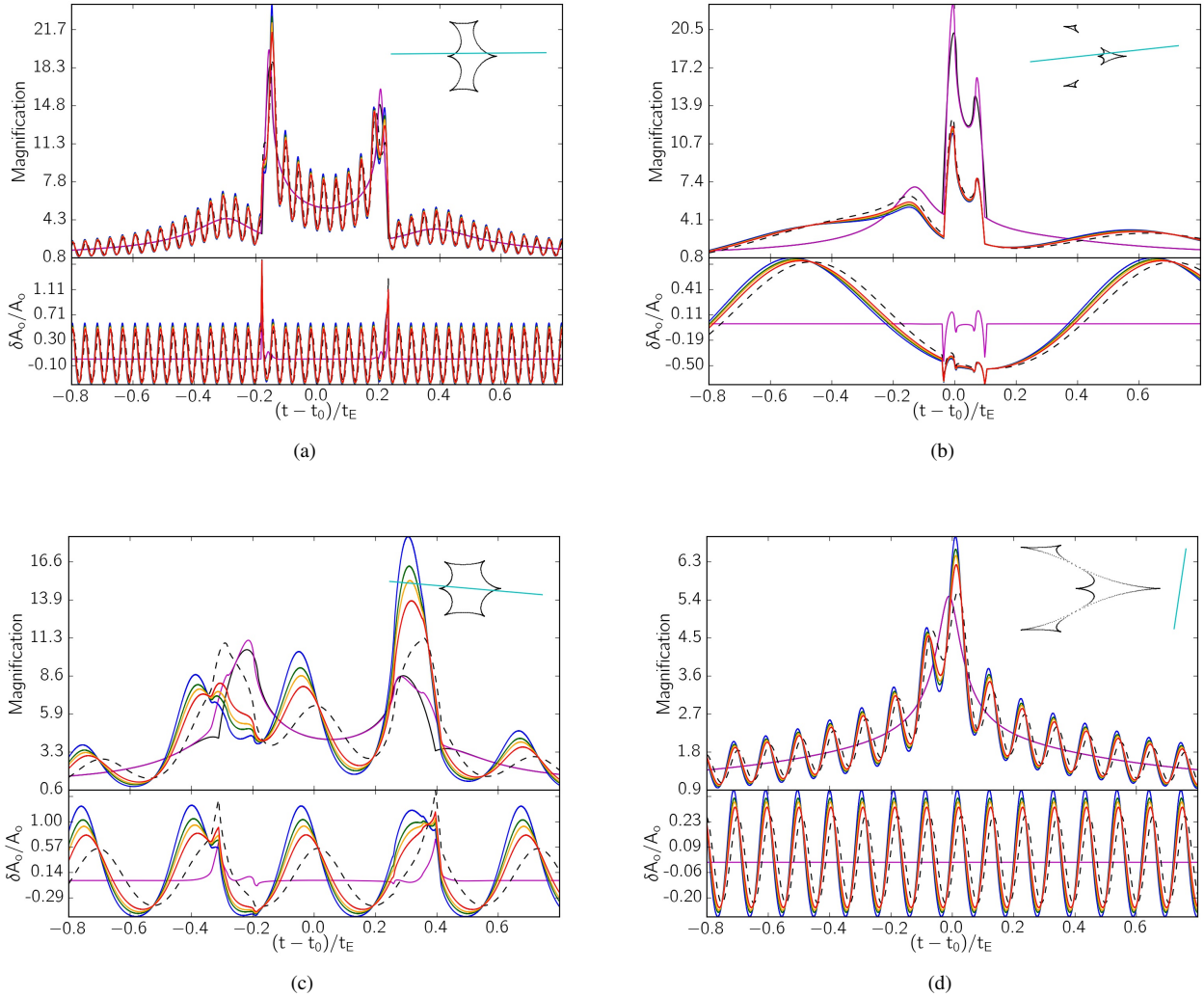


Figure 6. Examples of binary microlensing light curves from pulsing source stars. The parameters used to make each of them are listed in Table(1). More information about the plots can be found in the caption of Figure (5).

in Table (1). The three last columns of the Table are relevant for binary lenses but not single lenses: ξ is the angle of source trajectory relative to the binary axis in the lens plane, $d(R_E)$ is the binary distance normalized to the Einstein radius, and q is the ratio of the two stellar masses, respectively. Here we summarize several key aspects of the simulations.

(i) In binary microlensing from variable stars, the strongest effects occur during caustic crossing, owing to the variation in the finite source size, as emphasized with Figures 6(a) and 6(b). In residual panel, some deviations in the magenta solid curves develop right at the times of caustic crossings. The durations of these deviations are short, on the order of t_* for how the source takes to transit the caustic line. If $P \gg t_*$, the star is essentially of fixed angular extent during the caustic crossing. In that case discerning the periodic variability of the source radius during the crossing is difficult. If $P \sim t_*$ (either short period pulsations, or low lens-source relative proper motion, or large finite source size), then the effect of source variation is significant and can be discerned. Note that observational sampling of the light curve should be much shorter

than t_* . Certainly, the detection of variability in the source radius is more likely when t_* is long.

(ii) While fold crossing, the position of the maximum magnification depends on the source size. This point is demonstrated in Figure (7). The brightness peak during a fold-crossing changes position in response to the pulsational variation of the star, even for the magenta solid curves. When the source radius decreases, the peak becomes more slender and moves toward the fold line, and vice versa.

(iii) Generally the pulses of source stars have larger amplitudes while the magnification factor is high, as for example when the source is inside the caustic curve or when the source is quite close to the cusp of the caustic (see Figure 6(a)).

(iv) When the source is passing either close to the caustic line or tangential to it, an extended peak develops in light curve. Under these conditions, the variation of finite source size does not produce particularly remarkable deviations from a non-pulsing star (e.g., the magenta solid curves are over the solid black curves). One example is shown in Figure 6(b) around the time $0.2t_E + t_0$.

(v) If the pulsing amplitude is large $\delta T \sim 300$ K, the en-

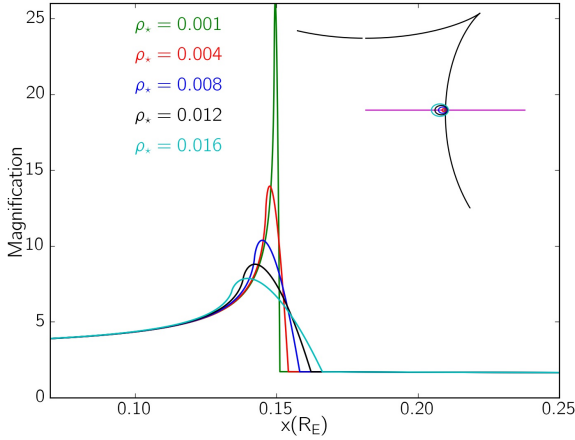


Figure 7. The magnification factor in binary caustic crossing versus the horizontal distance of the source center from the lenses' center of mass for several values of the source radius. The parameters used to make this plot are: $q = 1.0$, $d(R_E) = 1.0$ and $u_0 = 0.4$. The source trajectory is parallel with the binary axis.

hancements in the apparent brightness due to variability and lensing can be in the same order of magnitudes. In that case, the resulted light curve will be complicated, see, e.g. Figure 6(c). In these light curves, a significant displacement in the maximum magnification happens from the time of caustic-crossing.

(vi) In the absence of a caustic crossing (e.g., Fig. 6(d)), the deviation due to variable finite source size is negligible and other deviations are similar to single microlensing events with large impact parameter, such as magnifying several of the pulses.

5 SUMMARY AND CONCLUSIONS

Gravitational lensing has proven to be a powerful tool for study of the universe, ranging from macrolensing effects that have been used to study dark matter in galaxies and galaxy clusters, to microlensing phenomena for constraining dark matter candidates in the Milky Way halo. But microlensing has also been used as a probe of stellar astrophysics. For a close passage between a lensing mass and a background stellar source, differential magnification across the stellar source allows for a version of mapping the star. While this potential has been investigated theoretically for the effects of limb darkening, atmospheric polarization, and even circumstellar media, much less has been done to address the effects of stellar pulsation.

In this paper we consider specifically radially pulsating stars in the context of single-lens and binary-lens events. We adopt a simplified model for the pulsational behavior, as a sinusoidal variation in the radius and in the temperature (with a phase difference). For this initial study, we ignored limb darkening. For the single-lens case, we exploit this simple picture to deconstruct how different factors contribute to lensing light curves, including how the surface-averaged magnification factor varies with the changing source size, how the intrinsic source brightness changes with sources size, and how the stellar intensity changes with temperature variation.

The main outcomes from simulations of the single-lens mod-

els are as follows. Certainly when finite source effects are not important, the brightness variations from pulsational variability are simply mimicked in the lensing light curve. However, when the lens is quite near or transits the source, interesting effects occur, such as time-lag and amplitude differences for different passbands. Details regarding the strength of these effect depend on how the pulsation period, P , compares with duration of the lensing event, t_E , as well as how the pulsational phase (i.e., maximum or minimum brightness) compares to when the lens achieves its closest approach.

Binary lensing yields similar effects, although the magnification factor is more complex. The light curves in general now depend on the mass ratio of the lens, the binary separation, and the relative trajectory of the source in relation to the binary lens caustic pattern. As with the single-lens case, effects depend on the how the pulsation period compares with the duration of the lensing. Likewise, the observed brightness variation from pulsation can be strongly modified as compared to the unlensed case, and different curves can result for different passbands. For a single lens, the possibility of finite source effects is higher for stars of larger size, and small impact parameters are needed. For binary lenses the caustic structure is relatively larger, and caustic crossings always lead to high magnification effects, so finite source events are easier to detect for binary lenses.

An interesting distinction about the case of radial pulsators, as compared with finite source effects with non-pulsating stars, is the possibility of obtaining a good measurement for the source distance. When dealing with Galactic microlensing events, there can be degeneracies, such as the mass of the lens, the distance of the lens, the trajectory of the relative proper motion between the lens and source, and to some extent the distance to the source. The latter can be somewhat constrained. For example, in monitoring surveys of the LMC, the relative error for the source distance can be small, given that the LMC is much farther than its size. By contrast, there can be more ambiguity for the source distance when monitoring the Galactic Bulge. However, radial pulsators such as Cepheids and RR Lyrae stars are standard candles that follow a Leavitt Law relation for period of pulsation and luminosity. Consequently, microlensing that involves such a stellar source will provide an accurate determination of D_s .

In a second paper, we will explore the effects of non-radial pulsational (NRP) brightness variations on microlensing light curves. Overall, we can expect the amplitudes of intrinsic brightness variations to be lower than for radial pulsators. On the other hand, finite source effects from transits of the source by the lens should permit a determination of the trajectory of the transit relative to the principle axis of the star that defined the spherical harmonic l, m modes associated with the NRP variations. We also anticipate some sensitivity to stellar rotation in favorable cases.

ACKNOWLEDGEMENTS

RI acknowledges Ashton Morelock for preliminary calculations of single lens light curves of variable stars.

References

- Alcock C., et al., 2000, *ApJ*, **541**, 270
- Assef R. J., et al., 2006, *ApJ*, **649**, 954
- Benedict G. F., et al., 2002, *AJ*, **124**, 1695
- Bennett D. P., Rhie S. H., 1996, *ApJ*, **472**, 660

- Bond I. A., et al., 2001, *MNRAS*, **327**, 868
- Bozza V., 2010, *MNRAS*, **408**, 2188
- Bozza V., Bachelet E., Bartolić F., Heintz T. M., Hoag A. R., Hundertmark M., 2018, *MNRAS*, **479**, 5157
- Bryce H., 2001, PhD thesis, University of Glasgow
- Carroll B. W., Ostlie D. A., 1996, An introduction to modern astrophysics; 1st ed., Addison-Wesley, Reading, MA, <https://cds.cern.ch/record/642519>
- Catelan M., Smith H. A., 2015, Pulsating Stars
- Cox J. P., 1980, Theory of stellar pulsation
- Einstein A., 1936, *Science*, **84**, 506
- Fröhlich C., 2006, *Space Sci. Rev.*, **125**, 53
- Fu L.-P., Shu C.-G., 2005, Progress in Astronomy, **23**, 56
- Gaudi B. S., 2012, *ARA&A*, **50**, 411
- Gould A., 1994, *ApJ*, **421**, L71
- Gould A., Loeb A., 1992, *ApJ*, **396**, 104
- Hubble E., 1929, *Proceedings of the National Academy of Science*, **15**, 168
- Hubble E., Humason M. L., 1931, *ApJ*, **74**, 43
- Jetsu L., Porceddu S., 2015, *PLoS ONE*, **10**, 44140
- Kim D. J., et al., 2018, *AJ*, **155**, 76
- Kinman T. D., Brown W. R., 2010, *AJ*, **139**, 2014
- Li S. S., et al., 2019, *MNRAS*, **488**, 3308
- Majaess D. J., Turner D. G., Lane D. J., 2009, *MNRAS*, **398**, 263
- Mao S., Paczynski B., 1991, *ApJ*, **374**, L37
- Mróz P., et al., 2019, *ApJS*, **244**, 29
- Nemiroff R. J., Wickramasinghe W. A. D. T., 1994, *ApJ*, **424**, L21
- Paczynski B., 1986, *ApJ*, **301**, 503
- Pel J. W., 1985, in Madore B. F., ed., IAU Colloq. 82: Cepheids: Theory and Observation. pp 1–16
- Percy J. R., 2007, Understanding Variable Stars
- Pietrukowicz P., Latour M., Angeloni R., di Mille F., Soszyński I., Udalski A., Germanà C., 2015, *Acta Astron.*, **65**, 63
- Pietrukowicz P., et al., 2017, *Nature Astronomy*, **1**, 0166
- Saio H., 1993, *Ap&SS*, **210**, 61
- Samus N. N., Kazarovets E. V., Durlevich O. V., Kireeva N. N., Pastukhova E. N., 2009, VizieR Online Data Catalog, [p. B/gcvs](https://vizier.cern.ch/ftp/vizieR/online_data_catalog/p/B/gcvs)
- Samus N. N., Kazarovets E. V., Durlevich O. V., Kireeva N. N., Pastukhova E. N., 2017, *Astronomy Reports*, **61**, 80
- Schneider P., Ehlers J., Falco E. E., 1992, Gravitational Lenses, [doi:10.1007/978-3-662-03758-4](https://doi.org/10.1007/978-3-662-03758-4).
- Skowron J., Gould A., 2012, arXiv[astro-ph.EP]: 1203.1034,
- Skowron D. M., et al., 2019, *Science*, **365**, 478
- Soszyński I., et al., 2008, *Acta Astron.*, **58**, 163
- Turner D. G., 2010, *Ap&SS*, **326**, 219
- Udalski A., Soszyński I., Szymanski M., Kubiak M., Pietrzynski G., Wozniak P., Zebrun K., 1999, *Acta Astron.*, **49**, 223
- Wambsganss J., 2006, arXiv e-prints, [pp astro-ph/0604278](https://arxiv.org/abs/astro-ph/0604278)
- Witt H. J., Mao S., 1994, *ApJ*, **430**, 505
- Wyrzykowski Ł., et al., 2015, *ApJS*, **216**, 12
- Zhevakin S. A., 1963, *ARA&A*, **1**, 367